Micromechanical modelling of short fibre composites considering fibre length distributions

Composites Part B 264 (2023) 110868

Contents lists available at ScienceDirect

Composites Part B

journal homepage: www.elsevier.com/locate/composites

Micromechanical modelling of short fibre composites considering fibre length distributions

N. Mentges [a], H. Çelik [a], C. Hopmann [a], M. Fagerström [b], S.M. Mirkhalaf [c,*]

[a] Institute for Plastics Processing in Industry and Craft, RWTH Aachen University, Aachen, Germany
[b] Department of Industrial and Materials Science, Chalmers University of Technology, Gothenburg, Sweden
[c] Department of Physics, University of Gothenburg, Gothenburg, Sweden

ARTICLE INFO

Keywords:
Short fibre reinforced composites
Micromechanics
Fibre length distribution
Elasto-plastic behaviour

ABSTRACT

Mechanical response of short fibre composites is varying locally with respect to the microstructural constitution of the material, which in turn is a consequence of flow conditions during manufacturing. This local constitution is described by local fibre volume content, local fibre orientation distribution and local fibre length distribution. For short fibre reinforced plastics, both distributions are affected by flow conditions during an injection moulding process. Current material models for predicting the homogenised material response account for the local volume fraction and local fibre orientation distribution. Fibre length distribution, however, is usually approximated with a single average fibre length. To investigate the effects of fibre length distribution on the elasto-plastic response of short fibre composites, a micromechanical Orientation Averaging model has been extended. Two methods are presented in this work. In the first method, an additional averaging scheme over the fibre length distribution is included. In the second method, a novel representative fibre length is presented based on a stiffness-weighted average. The predictionsobtained from these methods are then compared and evaluated against experimental results of uniaxial tensile tests taken from literature. Good agreements are found using both methods. However, for the investigated behaviour, using a representative fibre length is still beneficial due to the superior computational performance.

1. Introduction

The use of short fibre reinforced composites (SFRCs) with thermoplastic polymer matrix in structural components increased in recent years. In addition to good mechanical properties, the material is an interesting choice for its highly efficient and economical production by injection moulding [1,2]. Besides the high requirements on the mechanical properties of SFRC structural components, the demand for lightweight solutions in modern transportation systems is increasing constantly. This results in a need for more reliable and accurate prediction on the response of these materials.

The local mechanical response of SFRCs is dependent on the local microscopic constitution of the composite. The local constitution is defined by fibre volume fraction, fibre orientation distribution and distribution of fibre length. These parameters are highly influenced by the locally varying flow conditions during the injection moulding process [3]. During processing, when polymer granulates are plasticised, fibre length degrades due to high stresses and also interaction of fibres with each other as well as with the screw walls [4]. During the injection phase, a radial flow forms in the area of the injection point. This causes fibres to orient themselves transversely to the flow direction. Due to the adhesion condition of the melt to the mould wall, shear flows occur in the surrounding area. This leads to a reorientation of the fibres parallel to the flow direction. From the described mechanisms, a fibre orientation distribution profile develops across the thickness of the component cross-section, where the fibres close to the mould cavity walls are oriented parallel to the flow direction and perpendicular in the centre [5]. Complex flow conditions in part geometries result in different layer structures. Fibre length distributions (FLDs) in SFRCs result from the high shear stresses in the material during the manufacturing process. Contact of the fibres with the screw or cavity walls and/or fibre-fibre interactions during the injection moulding process result in fibre breakage. Thus, the average fibre length can reduce to up to a tenth of the initial fibre length [4,6]. Consequently, the local constitution of injection moulded SFRC is strongly dependent on the processing properties such as temperature of the melt and mould cavity walls as well as the injection speed and the machine properties such as screw design.

* Corresponding author.
E-mail addresses: martin.fagerstrom@chalmers.se (M. Fagerström), mohsen.mirkhalaf@physics.gu.se (S.M. Mirkhalaf).

https://doi.org/10.1016/j.compositesb.2023.110868
Received 28 February 2023; Received in revised form 30 May 2023; Accepted 19 June 2023
Available online 28 June 2023

To take into account the local constitution of the composite material, micromechanical models have been developed. Such models for SFRCs are often based on mean field homogenisation methods such as the Mori–Tanaka-method [7]. A good overview on different mean field homogenisation methods is given in Pierrard [8]. Fibre orientation distribution (FOD) is then taken into account using an Orientation Averaging (OA) procedure, developed by Advani and Tucker [9]. The influence of the fibre orientation state is studied extensively. Different methods for describing the FOD in a parametric way have been investigated. Breuer et al. [10] compared different closure approximations for obtaining 4th and 6th order orientation distribution tensors from a 2nd order tensor and proposed a novel distribution function for the FOD based on the principle of maximum entropy. Al-Qudsi et al. [11] proposed an orthotropic closure approximation, which reaches higher prediction accuracy for elastic properties of SFRCs.

Mechanical response of SFRCs shows a strong dependence on the fibre length. Especially, the unidirectional composite stiffness in the fibre parallel direction is largely influenced by the fibre length. This is already demonstrated in common empirical models for the prediction of the unidirectional composite stiffness like the Halpin–Tsai-model. In the range of low fibre lengths, this relation is strongly nonlinear in the range of aspect ratios up to $l/d \leq 100$ [12]. By definition, SFRCs contain fibre aspect rations of up to 100 [5]. Hence, the distribution of aspect ratios of the fibres is mainly within this range. Consequently, the influence of fibre length distributions must be considered in the modelling of short fibre composites.

In the linear elastic case, FLDs and their effect on the response of SFRCs have been studied extensively. In most cases, the distribution of fibre lengths is found to follow a Weibull distribution [13–15]. However, Lee et al. [16] mention the logarithmic Generalised Extreme Value distributions as other possible probability density function. Fu and Lauke [17] used a laminate analogy approach to investigate the effect of theoretical probability distribution functions for fibre orientation and fibre length on the resulting mechanical composite properties. Besides the dependency of the stiffness of the shape of the orientation distribution and the mean orientation, they found a significant effect of the fibre length distribution on the resulting composite stiffness. They showed that not only the mean fibre length, but also the modal values of the FLD affect the resulting composite stiffness significantly. Hine et al. [18,19] investigated different single averaged fibre length from an FLD to approximate the full distribution. In their investigations, the number-averaged fibre length is found to give an adequate estimation for a single representative fibre length. In fact, using the number-averaged fibre length as representation of an FLD is a commonly used method for predicting the response of SFRCs [20,21].

To the authors' knowledge, the effect of FLDs on the non-linear response of SFRCs has not been studied in the literature so far. Micromechanics-based models proposed by Sasayama et al. [22] and Notta-Cuvier et al. [23] take into account the effect of fibre length on the elasto-plastic and damage response of the materials. However, the effect of the distributions of fibre lengths is not considered in the calculations. In fact a number averaged fibre length is used in both cases.

Hence, in this study, the effect of FLDs on the non-linear elasto-plastic behaviour of SFRCs is investigated. Therefore, the two-step OA method for the elasto-plastic response of SFRCs developed by Mirkhalaf et al. [24] is extended to include the effects of FLDs. Two different methods for implementing the FLD into the model are investigated. One is using an additional averaging scheme over the FLD, and the other uses a single representative fibre length.

The remaining of this paper is structured as follows. The general methodology of the two-step OA method for the elasto-plastic response of SFRCs is outlined in Section 2. Based on this method, the extension to consider FLDs within the OA procedure using an additional averaging scheme is discussed in Section 3. In sub- Section 3.2, the reduction to a single representative fibre length and the novel representative fibre length based on the stiffness–weighted average are presented. In Section 4, model predictions from both methods are obtained using experimental results taken from literature. The model predictions are additionally compared to each other and to the experimental results. Finally, conclusions from these investigations are given in Section 5.

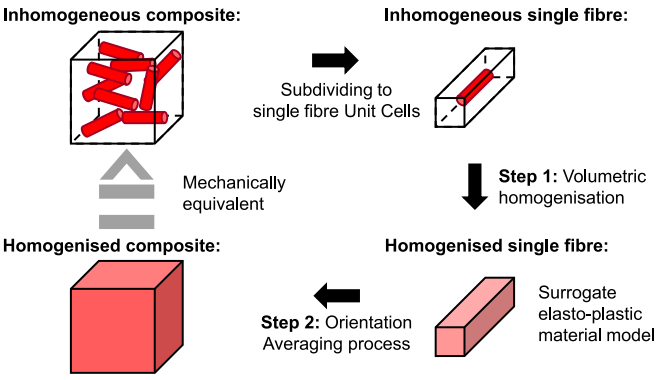

Fig. 1. Schematic overview of the two-step OA method [24].

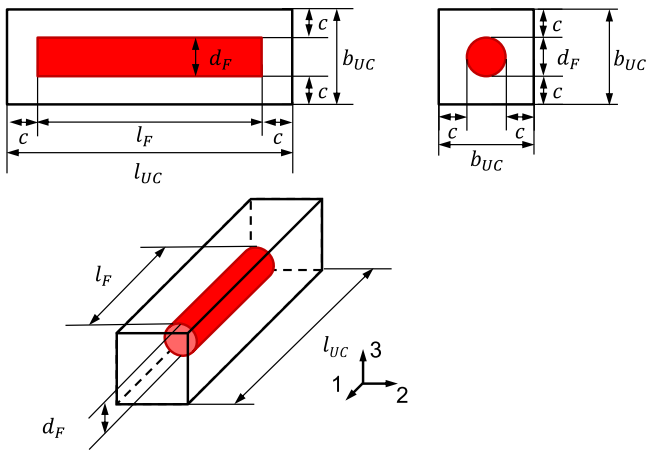

Fig. 2. Geometry of a single fibre Unit Cell.

2. The two-step orientation averaging model

In this section, the two-step Orientation Averaging (OA) method, developed by Mirkhalaf et al. [24], is explained. The model incorporates two homogenisation steps and uses Finite Element Analysis (FEA) and Orientation Averaging [9]. This model is an extention to an FE-based two-step OA model for elastic properties of SFRCs [25]. Castricum et al. [26,27] have employed the model together with Finite Element Method (FEM) and developed a coupled multi-scale (macro–micro) model. Fig. 1 shows a schematic workflow of the model and its homogenisation steps. Starting from a local configuration of the inhomogeneous composite, first, a single isolated fibre embedded in matrix is investigated. In a volumetric homogenisation procedure, the homogenised material response of the unit cell (UC) including a single fibre is obtained. Subsequently, on the global level (composite level), Fibre Orientation Distribution (FOD) is introduced in the OA step.

2.1. Numerical homogenisation of a single fibre unit cell

Homogenisation of a single fibre UC is conducted to obtain homogenised mechanical properties of the unidirectional (UD) composite.

For this, analytical methods can be used. Many of those are categorised under the class of mean-field homogenisation methods. In these methods, a fibre is modelled as an ellipsoidal inclusion surrounded by the matrix material. Examples for these methods are the Mori–Tanaka–model [7] and the double inclusion model by Hori and Nemat-Nasser [28,29]. Mean-field homogenisation methods show good capabilities in predicting the linear elastic response of SFRC [8]. However, when it comes to nonlinear effects such as matrix yielding or even material damage, many analytical models yield inaccurate predictions of the homogenised material response. Therefore, Mirkhalaf et al. [24,25] use numerical simulations (Finite Element Analysis) of a single fibre UC for the first step of the OA method. This method is also used in this work. The Finite Element (FE) model consists of a cylindrical fibre placed in the centre of a UC, a cuboid of matrix with a quadratic cross-section perpendicular to fibre direction. The dimensions of the UC are defined by the fibre dimensions, d_F, l_F and the fibre volume fraction φ. Additionally, the UC response is strongly dependent on the UC length relative to the fibre length. Investigations on these effects have shown that using an equidistant spacing between the fibre and UC boundaries in all directions results in a good estimation of homogenised unidirectional material properties. Using this spacing is also proposed by Modniks, Andersons [21]. With the distance between fibre and UC-boundaries represented by c, the fibre volume fraction can be defined as follows:

$$\varphi = \frac{\pi}{4} \frac{l_F \, d_F^2}{\left(l_F + 2c\right)\left(d_F + 2c\right)^2}. \tag{1}$$

A visualisation of a UC geometry is given in Fig. 2. The fibre material is usually modelled as a linear elastic material. However, different material models may be used for the matrix material and for the fibre–matrix interface. Periodic Boundary Conditions (PBC) are applied on the UC walls. In order to obtain a complete view of the idealised transversal isotropic material behaviour, four independent load cases need to be applied [24]. Two uniaxial stresses (parallel and perpendicular to the fibre direction) and two shear loading cases are used in this work. Using the obtained FE results, a transverse isotropic elasto-plastic surrogate model is calibrated [24]. With the help of this surrogate model, not only the investigated basic stress states, but also complex and multiaxial stress states can be represented without the need for additional FE simulations. The calibrated surrogate constitutive model is then used in an incremental framework. In each load increment, the model gives the response of the homogenised UC to any arbitrary loading state. The model, following Runesson et al. [30], is formulated under the assumption of small strains. It consists of a reduced transverse isotropic linear elastic model combined with a simplified transverse isotropic version of the Hill's yield criterion. The elastic stiffness tensor $\mathbb{C}_U^e$ is defined by

$$\mathbb{C}_U^e = \mathbb{C}_U^{e,iso} + (C-1)\,(2G+L)\,\mathbf{A}\otimes\mathbf{A}, \tag{2}$$

where $\mathbb{C}_U^{e,iso}$ represents an isotropic stiffness tensor with independent parameters defined by the Young's modulus E and Poisson's ratio ν. Furthermore, $\mathbf{A}$ is a second order structural tensor, representing the fibre orientation $\mathbf{p}$ in the UC with $\mathbf{A} = \mathbf{p}\otimes\mathbf{p}$. In this study, the fibre is oriented in the 1-direction of the UC. Hence, the tensor is defined as $\mathbf{A} = diag(1,0,0)$. Finally, the model parameter C in Eq. (2) introduces the transversal isotropy. In case of $C = 1$, the standard isotropic stiffness tensor is obtained [30].

The Hill's yield function Φ_U for a simplified transverse isotropic case reads

$$\Phi_U = \frac{1}{(1-R)\sigma_y^2}\left[R\left[\sigma_{U,22}-\sigma_{U,33}\right]^2 + \left[\sigma_{U,11}-\sigma_{U,22}\right]^2 + \left[\sigma_{U,11}-\sigma_{U,33}\right]^2\right] + \frac{2(2R+1)}{(R+1)\sigma_y^2}\left[\sigma_{U,12}^2+\sigma_{U,23}^2+\sigma_{U,13}^2\right] - \alpha(\bar{\varepsilon}_U^p), \tag{3}$$

where σ_{ij} represents the components of the Cauchy stress tensor, σ_y defines the yield stress for uniaxial stress in the isotropic plane, and parameter R is defined by the relation of the uniaxial yield stress in fibre direction to the perpendicular yield stress σ_y. This causes the transversal isotropy in the yield criterion. For $R = 1$, the von Mises yield criterion is obtained. Finally, α defines the hardening behaviour of the material model defined in this study by an isotropic hardening rule given by a third order polynomial:

$$\alpha(\bar{\varepsilon}_U^p) = 1 + H_1\bar{\varepsilon}_U^p + H_2(\bar{\varepsilon}_U^p)^2 + H_3(\bar{\varepsilon}_U^p)^3, \tag{4}$$

where $\bar{\varepsilon}_U^p$ represents an effective accumulated plastic strain, and H_1, H_2 and H_3 are the hardening parameters. In summary, the surrogate model is defined by (I) a simplified transverse isotropic linear elastic law, and (II) a transverse isotropic Hill's criterion, and (III) an isotropic hardening following a polynomial rule. The linear elastic material behaviour is defined by the isotropic engineering constants E and ν and an anisotropy coefficient C. The yield criterion is defined by the two parameters σ_y and R, and the hardening rule consists of three parameters H_1, H_2 and H_3 to be calibrated. Consequently, eight independent model parameters must be calibrated from the numerical simulations of the single fibre UC.

2.2. Incorporating fibre orientation distribution

In the second step of the original model, FOD is applied by an averaging scheme. For this, the local UC-stress state $\boldsymbol{\sigma}_U^L$ is transformed to the global composite coordinate system. For this, a coordinate transformation is conducted using a rotational tensor $\mathbf{R}$:

$$\mathbf{e}_i^L = \mathbf{R}\cdot\mathbf{e}_i, \tag{5}$$

where $\mathbf{e}_i$ and $\mathbf{e}_i^L$ represent the global and local orthonormal base vectors, respectively. In this work, $\mathbf{e}_1^L$ is the fibre direction at the local coordinate system. The UC stress at the global configuration is given by

$$\boldsymbol{\sigma}_U = \left[\mathbf{R}^T(\mathbf{p}) \,\overline{\otimes}\, \mathbf{R}^T(\mathbf{p})\right] : \boldsymbol{\sigma}_U^L. \tag{6}$$

where $\boldsymbol{\sigma}_U^L$ is the UC stress at the local configuration, and the operator $\overline{\otimes}$ denotes the non-standard open product with $(\mathbf{A}\,\overline{\otimes}\,\mathbf{B})_{ijkl} = \mathbf{A}_{ik}\mathbf{B}_{jl}$. The homogenised composite stresses $\boldsymbol{\sigma}_C$ is obtained by a weighted integration over the unit sphere:

$$\boldsymbol{\sigma}_C = \oint \left[\mathbf{R}^T(\mathbf{p}) \,\overline{\otimes}\, \mathbf{R}^T(\mathbf{p})\right] : \boldsymbol{\sigma}_U^L(\mathbf{p})\,\psi(\mathbf{p})\,\mathrm{d}\mathbf{p}. \tag{7}$$

The weighting is defined by the FOD-function $\psi(\mathbf{p})$ (with $\oint_\Omega \psi(\mathbf{p})\,\mathrm{d}\mathbf{p} = 1$). The rotation tensor $\mathbf{R}$ is solely dependent on the fibre orientation vector $\mathbf{p}$.

Remark 1. In some cases, the FOD is represented in the form of a second order tensor $\mathbf{a}$, defined by [9]:

$$\mathbf{a} = \oint \mathbf{p}\otimes\mathbf{p}\,\psi(\mathbf{p})\,\mathrm{d}\mathbf{p}. \tag{8}$$

The inverse transformation to a FOD-function ψ is not unambiguous. An infinite number of distribution functions can be found which represent the same FOD-tensor. Hence, certain assumptions must be taken to further specify the shape of the function. In this work the maximum entropy approach is chosen, based on the work of Breuer et al. [10]. The method is based on the assumption that the FOD generally takes the form of maximum disorder within the given FOD-tensor. That assumption results in an FOD-function based on a normal distribution on a unit sphere, the Bingham distribution [10,31].

Due to the non-linearity of the problem, the rate form of Eq. (7) is used:

$$\dot{\boldsymbol{\sigma}}_C = \oint \left[\mathbf{R}^T(\mathbf{p}) \,\overline{\otimes}\, \mathbf{R}^T(\mathbf{p})\right] : \dot{\boldsymbol{\sigma}}_U^L(\mathbf{p})\,\psi(\mathbf{p})\,\mathrm{d}\mathbf{p}, \tag{9}$$

which results in an incremental formulation:

$$\Delta\boldsymbol{\sigma}_C = \oint \left[\mathbf{R}^T(\mathbf{p}) \,\overline{\otimes}\, \mathbf{R}^T(\mathbf{p})\right] : \Delta\boldsymbol{\sigma}_U^L(\mathbf{p})\, \psi(\mathbf{p})\, \mathrm{d}\mathbf{p}. \tag{10}$$

In order to define the local (UC) strain state (in relation to the composite strain state), three different interaction assumptions are used. These global–local interactions include Voigt (V), Reuss (R) and self-consistent (SC) assumptions. The Voigt interaction assumption is based on postulation of uniform strain and results in upper bound predictions:

$$\Delta\boldsymbol{\varepsilon}_U^L = \left[\mathbf{R}(\mathbf{p}) \,\overline{\otimes}\, \mathbf{R}(\mathbf{p})\right] : \Delta\boldsymbol{\varepsilon}_C. \tag{11}$$

From the local strain state, the local stress state is computed using the calibrated surrogate model. Subsequently, the homogenised composite stress is obtained using Eq. (10). Additionally, the tangential stiffness tensor (for the Voigt interaction) is obtained by

$$\mathbb{C}_C^V = \oint \left[\mathbf{R}^T(\mathbf{p}) \,\overline{\otimes}\, \mathbf{R}^T(\mathbf{p})\right] : \mathbb{C}_U^L : \left[\mathbf{R}(\mathbf{p}) \,\overline{\otimes}\, \mathbf{R}(\mathbf{p})\right]\, \psi(\mathbf{p})\, \mathrm{d}\mathbf{p}. \tag{12}$$

The Reuss interaction assumption presumes a uniform stress state and results in a lower bound prediction:

$$\Delta\boldsymbol{\sigma}_U^L = \left[\mathbf{R}(\mathbf{p}) \,\overline{\otimes}\, \mathbf{R}(\mathbf{p})\right] : \Delta\boldsymbol{\sigma}_C. \tag{13}$$

In a strain induced loading procedure, first, the composite stress increment must be obtained using the tangential composite stiffness from the previous strain increment:

$$\Delta\boldsymbol{\sigma}_C = \mathbb{C}_C^R : \Delta\boldsymbol{\varepsilon}_C, \tag{14}$$

with

$$\mathbb{C}_C^R = \left\{ \oint \left[\mathbf{R}^T(\mathbf{p}) \,\overline{\otimes}\, \mathbf{R}^T(\mathbf{p})\right] : \left[\mathbb{C}_U^L\right]^{-1} : \left[\mathbf{R}(\mathbf{p}) \,\overline{\otimes}\, \mathbf{R}(\mathbf{p})\right]\, \psi(\mathbf{p})\, \mathrm{d}\mathbf{p} \right\}^{-1}. \tag{15}$$

The self-consistent interaction relies on a more complex assumption and is an intermediate approach between the Voigt and Reuss assumptions. Here, each UC is considered as an inclusion in an *equivalent homogeneous medium* with composite properties. For this interaction, the UC strain increment is given by

$$\Delta\boldsymbol{\varepsilon}_U = \left[\mathbb{I} + \mathbb{E} : \left(\left[\mathbb{C}_C^{SC}\right]^{-1} : \mathbb{C}_U - \mathbb{I}\right)\right]^{-1} : \Delta\boldsymbol{\varepsilon}_C, \tag{16}$$

where $\mathbb{I}$ represents the fourth order identity tensor, $\mathbb{E}$ is the fourth order Eshelby tensor for anisotropic media which is dependent on the composite stiffness tensor [32], and $\mathbb{C}_U$ is the UC tangent stiffness tensor in global coordinates given by

$$\mathbb{C}_U = \left[\mathbf{R}^T(\mathbf{p}) \,\overline{\otimes}\, \mathbf{R}^T(\mathbf{p})\right] : \mathbb{C}_U^L : \left[\mathbf{R}(\mathbf{p}) \,\overline{\otimes}\, \mathbf{R}(\mathbf{p})\right], \tag{17}$$

In Eq. (16), $\mathbb{C}_C^{SC}$ represents the homogenised tangent composite stiffness tensor using the self-consistent interaction assumption:

$$\mathbb{C}_C^{SC} = \oint \mathbb{C}_U : \left[\mathbb{I} + \mathbb{E} : \left(\left[\mathbb{C}_C^{SC}\right]^{-1} : \mathbb{C}_U - \mathbb{I}\right)\right]^{-1}\, \psi(\mathbf{p})\, \mathrm{d}\mathbf{p}. \tag{18}$$

Note that a self-dependency occurs for Eq. (18). This equation is solved using a fixed point iteration algorithm. The local UC strain is obtained by

$$\Delta\boldsymbol{\varepsilon}_U^L = \left[\mathbf{R}(\mathbf{p}) \,\overline{\otimes}\, \mathbf{R}(\mathbf{p})\right] : \Delta\boldsymbol{\varepsilon}_U. \tag{19}$$

It should be mentioned that the presented Unit Cell model is an idealisation of the actual microsructure in an SFRC. Using this UC model, the effects of stress concentrations, caused by surrounding fibres, on the macroscopic mechanical response are not accounted for. These effects are particularly relevant for damage initiation and failure. Also, stress concentrations from local fibre–fibre interactions would affect the matrix yielding, and in turn, the macroscopic yielding behaviour of the composite. Using multi-fibre realistic representative volume elements (RVEs), fibre–fibre interactions will be taken into account more precisely. However, this approach has a considerably higher computational cost. Mirkhalaf et al. [24] conducted a comparative study between the two-step OA approach and RVE computational homogenisation, and the OA method showed a remarkably better computational performance. It should also be emphasised that interactions between UCs are implicitly incorporated into the self-consistent interaction through the calculation of the Eshelby tensor.

For a more elaborated discussion about the original two-step homogenisation method, an interested reader is referred to [24]. The presented original model and all further extensions have been implemented using Python, and the presented results are all obtained from these implementations.

3. Incorporating fibre length distributions in the two-step OA method

Using an average fibre length instead of considering the fibre length distribution is proven to deliver good predictions in the linear elastic regime [18,20]. However, when elasto-plastic effects are included, the influence of fibre length distributions could potentially be considerable on the composite response. In the following, different methods for incorporating FLDs are discussed.

3.1. A second integration over FLD

To extend the OA model for considering FLDs, a second averaging integration is added to the homogenised stress increment calculation in Eq. (10):

$$\Delta\boldsymbol{\sigma}_C = \int_0^\infty \oint \left[\mathbf{R}^T(\mathbf{p}) \,\overline{\otimes}\, \mathbf{R}^T(\mathbf{p})\right] : \Delta\boldsymbol{\sigma}_U^L(l_F)\, \psi(\mathbf{p}, l_F)\, \mathrm{d}\mathbf{p}\, w(l_F)\, \mathrm{d}l_F, \tag{20}$$

where l_F represents the fibre length and $w(l_F)$ is the volume weighted fibre length distribution given in dependence of the unweighted fibre length distribution $f(l_F)$ as

$$w(l_F) = \frac{f(l_F)\, l_F}{\int_0^\infty f(l_F)\, l_F\, \mathrm{d}l_F}, \tag{21}$$

with $\int_0^\infty w(l_F)\, \mathrm{d}l_F = 1$. In practice on a measured and discrete FLD, the integration over the fibre lengths is performed between the minimum and maximum measured fibre lengths. The composite stiffness is then given by

$$\mathbb{C}_C^V = \int_0^\infty \oint \left[\mathbf{R}^T(\mathbf{p}) \,\overline{\otimes}\, \mathbf{R}^T(\mathbf{p})\right] : \mathbb{C}_U^L(l_F) : \left[\mathbf{R}(\mathbf{p}) \,\overline{\otimes}\, \mathbf{R}(\mathbf{p})\right]\, \psi(\mathbf{p}, l_F)\, \mathrm{d}\mathbf{p}\, w(l_F)\, \mathrm{d}l_F. \tag{22}$$

Note that, based on Fubini's theorem, the integrations over fibre length and orientation distribution are interchangable.

This extension with an additional averaging scheme has two major consequences for the realisation of the OA procedure in the material model. In the first step of the OA method, the whole range of fibre lengths must be considered. Since numerical simulations are used for obtaining the homogenised unidirectional response of a UC, only discrete fibre lengths can be considered for the fibre length dependent material behaviour. Hence, the FLD must be projected on discrete fibre lengths from which the homogenised response can be obtained in independent numerical simulations. This approach results in an increased computational effort when calculating the fibre length dependent material response. Another consequence concerns the second step of the OA procedure. The additional averaging scheme results in higher calculation times due to the number of iterations that need to be conducted. The increased computational cost correlates with the number of discrete fibre lengths considered. This effect is especially relevant for the SC interaction, since its calculation of the composite stiffness contains a fixed-point iteration.

3.2. Reduction to a single representative fibre length

As mentioned in Section 3.1, incorporating another integration over FLD in the two-step OA method results in a computationally expensive model. Hence, another approach which is basically reduction of the fibre length distribution to a single representative fibre length, is derived from the previous method and examined. In Eq. (22), the FOD-function ψ is marked as dependent on the fibre length. This dependency can be detected using micro-CT-scans of SFRC specimens [33]. However, in most literature, a dependency of the FOD on the fibre length is neglected. Following this approach, the equations for composite stiffness using the Voigt interaction assumption can be rearranged to isolate the integral over the fibre length to the UC-stiffness

$$\mathbb{C}_C^V = \oint \left[\mathbf{R}^T(\mathbf{p}) \,\overline{\otimes}\, \mathbf{R}^T(\mathbf{p})\right] : \left\{ \int_0^\infty \mathbb{C}_U^L(l_F)\; w(l_F)\; \mathrm{d}l_F \right\} : \left[\mathbf{R}(\mathbf{p}) \,\overline{\otimes}\, \mathbf{R}(\mathbf{p})\right]\; \psi(\mathbf{p})\; \mathrm{d}\mathbf{p}. \tag{23}$$

Note that this simplification is only fully applicable for the linear elastic case, since in the elasto-plastic regime, the material response is dependent on the loading history, and thus, UC tangent stiffness in each load increment depends on the previous increment. The inner integral of this equation (integral in the curly brackets) can be interpreted as fibre length averaged composite stiffness. Note that for the linear elastic case, the integral is fully independent of the fibre orientation **p**. Following the general assumption in e.g. [12] that, at constant fibre volume fraction, the unidirectional UC-Young's modulus is only dependent on the fibre length in fibre direction ($E_{11}(l_F)$), only the fibre parallel component must be calculated in the fibre length averaging. The assumption also implies that a single representative fibre length l_F^{rep} can be found from this relation, for which the UC-stiffness is equivalent to the fibre length averaged composite stiffness

$$E_{11}^{UC} = \int_0^\infty E_{11}^{UC}(l_F)\; w(l_F)\; \mathrm{d}l_F \;\equiv\; E_{11}(l_F^{rep}). \tag{24}$$

It is emphasised that replacing the FLD with a single representative fibre length is not a new concept in modelling SFRC. Often a number-averaged or volume-averaged fibre length is considered [18,20]. Especially the number-averaged fibre length is found to produce good estimations of a homogenised material response. However, these are empirical relations and are not necessarily applicable on fibre length distributions varying from the classical Weibull distribution form. This may exemplarily be the case in [34], where a bimodal fibre length distribution is found.

3.3. Stiffness weighted representative fibre length

As mentioned before, none of the commonly used representative fibre lengths directly takes into account the nonlinear effects of the fibre length on the mechanical properties. Hence, in this work, another representative fibre length is derived directly from Eq. (24). Replacing the volume weighted FLD with Eq. (21) results in

$$E_{11}(l_F^{rep}) = \frac{\int_0^\infty E_{11}^{UC}(l_F)\; l_F\; f(l_F)\; \mathrm{d}l_F}{\int_0^\infty l_F\; f(l_F)\; \mathrm{d}l_F}. \tag{25}$$

This is a averaging method which obtains an average homogenised stiffness value. However, an averaged representative fibre length is required here. Replacing the fibre length l_F in the denominator of the integral by the fibre parallel composite Young's modulus $E_{11}^{UC}(l_F)$ changes the result into a length value

$$l_F^{stiff} = \frac{\int_0^\infty l_F\; E_{11}^{UC}(l_F)\; f(l_F)\; \mathrm{d}l_F}{\int_0^\infty E_{11}^{UC}(l_F)\; f(l_F)\; \mathrm{d}l_F}, \tag{26}$$

which can be interpreted as a stiffness-averaged fibre length l_F^{stiff}. Noteworthy is that this fibre length directly takes into account the UC-Young's modulus.

Obtaining the stiffness-averaged fibre length from numerical simulations is not practical, since performing UC simulations for each fibre length class would result in high computational costs. However, the linear elastic properties can be calculated analytically in a good approximation using analytical models. Mean field homogenisation methods could be used here. In this work, however, an empirical model, the Halpin–Tsai-model [12] is used for estimating the fibre parallel UC-stiffness. The model gives a very good approximation of the fibre length dependent UC-stiffness using a simple relation, with

$$E_{11}^{UC} = \frac{1 + 2(l_F/d_F)\;\eta\;\phi}{1 - \eta\;\phi}\; E_M, \tag{27}$$

$$\eta = \frac{E_F/E_M - 1}{E_F/E_M + 2\;(l_F/d_F)}. \tag{28}$$

This provides an easy and efficient way to calculate the stiffness-averaged fibre length. Using a representative fibre length may lead to a significant reduction of computational time compared to the fibre length averaging extension, as described earlier. However, this comes with a loss of information on the local fibre length dependent material behaviour. In the linear elastic domain, this effect might still be fully represented when using the stiffness-averaged fibre length. However, concerning elasto-plastic effects or even material damage at a later point, the applicability still needs to be investigated numerically.

In total, two differing methods for considering fibre length distributions are presented. First, an additional averaging scheme is used to incorporate the fibre length distributions in the second step of the OA method. This approach will be referred to as method 1. Secondly, in method 2, the fibre length distribution is already considered in the first step of OA. Here, a representative fibre length is calculated using different weighting methods. An overview of the two different methods is given in Fig. 3.

4. Simulations and comparisons to experiments

In this section, simulations are conducted using the developed methods for representing fibre length distributions in SFRCs. Also, comparisons between the model predictions and experimental results, taken from literature, are performed. For the representative fibre length approach, three different methods discussed in the previous section (number-, volume-, and stiffness-averaged) are investigated.

4.1. Material properties and surrogate model calibrations

A glass fibre reinforced Polyamide 6 is investigated for which experimental results are taken from Holmstroem et al. [35,36]. Quasi-static tests were performed on two SFRCs with different mass contents of E-glass fibre (15 and 30%wt.) and also pure polymeric samples from the matrix material. The two different SFRCs will be referred to as PA-GF15 and PA-GF30 considering the respective mass content. On the matrix material tests, we have calibrated an isotropic elasto-plastic material model using J_2-plasticity with isotropic linear hardening defined by a hardening modulus K. The linear elastic matrix-properties have been obtained directly from [35]. Model parameters for the plasticity model have been calibrated based on the data provided in [36] using a gradient descent optimisation. The Experimental results together with the predictions using the calibrated model is shown in Fig. 4. For the fibre properties, standard values, taken from [37], are used. The calibrated material parameters for the matrix and fibre properties are given in Table 1. Also, additional properties of the composites (fibre content, fibre geometry, and fibre orientation distribution) for the two different SFRCs are given in Table 2. The fibre orientation state is given in the form of the second order fibre orientation distribution tensor **a** in diagonal form with the 11-entry representing the orientation in flow direction during the production process and 33 representing the through thickness direction. Due to the manufacturing process, a layered structure of fibre orientations is present in the specimen

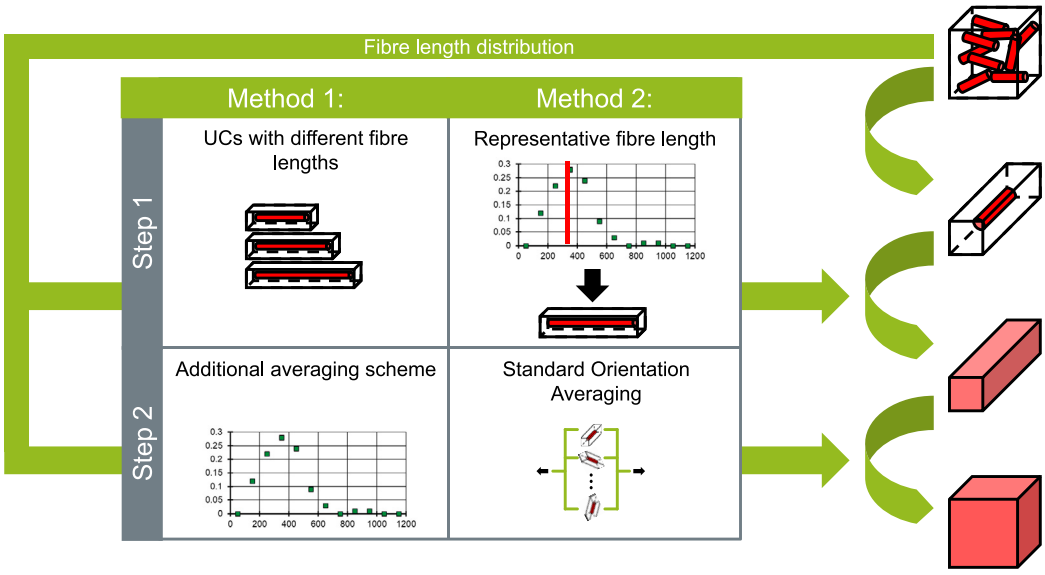

Fig. 3. Schematic overview on the two methods for incorporating FLD in the OA method.

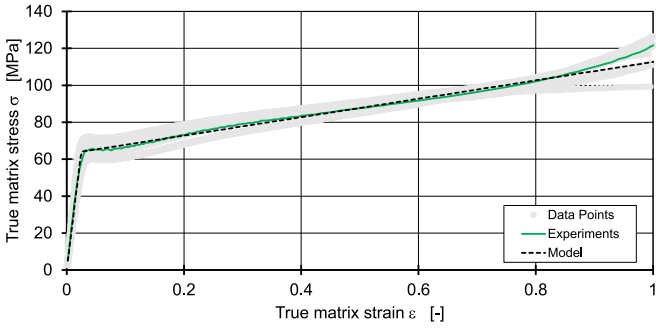

Fig. 4. Stress–strain curves of the PA6 matrix material provided by [35] and the calibrated material model.

Table 1
Mechanical properties of the constituents of the studied composite materials.

Property	Young's modulus	Poisson's ratio	Yield stress	Hardening modulus
Unit	[MPa]	[–]	[MPa]	[MPa]
Matrix	2800	0.4	64.1	50.8
Fibre	70,000	0.2	–	–

which is neglected in this case. The authors [35,36] obtained the fibre orientation state via micro-CT scans and deliver information on the development of the fibre orientation through the plate thickness. However, in this work, an averaged orientation state through the thickness is considered. The FLDs of the two materials are given in Fig. 5.

In order to obtain the elasto-plastic response of each relevant fibre length class (needed for method 1), 12 independent single fibre UCs are investigated numerically using four independent stress states. Subsequently, the surrogate model calibrations are performed based on the simulations for each fibre length. The material parameters in the surrogate model are calibrated using an optimisation process. The large number of parameters in this model reduces the chance of finding a global minimum in the optimisation procedure. To increase the possibility of obtaining physically realistic parameters after optimisation, the calibration process is conducted in three separate steps:

1. First, the linear elastic model, Eq. (2), is calibrated using the linear elastic regime of the four independent UC simulations up to a strain load of 0.3%.
2. In the second step, the yield point σ_y is obtained from the normal stress simulation in fibre perpendicular direction following the 0.2%-offset rule [38].
3. In the last step, the post-yielding domain of the UC behaviour is used for the calibration of the anisotropic yielding parameter R and the hardening parameters H_1, H_2 and H_3).

For the calibration steps 1 and 3, an objective function, given in Eq. (29), is defined in form of the sum of mean squared errors (MSE) for stresses and strains for the four independent load case by:

$$\epsilon_{fit} = \sum_{n=1}^{4} \left(\frac{\int_0^{T_n} \left\| \boldsymbol{\sigma}_n^{sim}(t) - \boldsymbol{\sigma}_n^{model}(t) \right\|^2 \mathrm{d}t}{\int_0^{T_n} \left\| \boldsymbol{\sigma}_n^{sim}(t) \right\|^2 \mathrm{d}t} + \frac{\int_0^{T_n} \left\| \boldsymbol{\varepsilon}_n^{sim}(t) - \boldsymbol{\varepsilon}_n^{model}(t) \right\|^2 \mathrm{d}t}{\int_0^{T_n} \left\| \boldsymbol{\varepsilon}_n^{sim}(t) \right\|^2 \mathrm{d}t} \right), \tag{29}$$

with n representing the 4 load cases and T_n representing each time increment of the simulated load cases. In Eq. (29), $\|\mathbf{X}\|$ represents the tensor norm defined as $\|\mathbf{X}\| := \sqrt{\mathbf{X} : \mathbf{X}} = \sqrt{X_{ij} X_{ij}}$. This objective function is minimised in the calibration steps using a downhill simplex method (implemented in Python with the Numpy library) in order to obtain optimal material parameters for the surrogate model. The corresponding surrogate model parameters for the two SFRCs with different fibre volume contents are given in Appendix A. In Fig. 6, an exemplary surrogate model fit on the FE simulations of a UC is given for the PA-GF15 composite with a fibre length of 1150 μm. A good correlation is found in all load cases in the linear elastic domain as well as in the elasto-plastic domain. In this particular calibration, for the linear elastic domain, $\epsilon_{fit}^{el} = 3.891 \times 10^{-3}$ is obtained and for the elasto-plastic domain $\epsilon_{fit}^{pl} = 1.049 \times 10^{-2}$ is found.

For method 2, corresponding representative fibre lengths, obtained from the FLDs [36], are given in Table 3. It can be noted that the stiffness-averaged fibre length produces an intermediate value between the number- and the volume-averaged with the stiffness-averaged being much closer to the number-averaged fibre length. For corresponding surrogate model parameters and MSE values, the reader is referred to Appendix A.

4.2. Linear elastic results

First, linear elastic predictions are obtained, and the two modelling approaches are compared to each other and experimental results. In

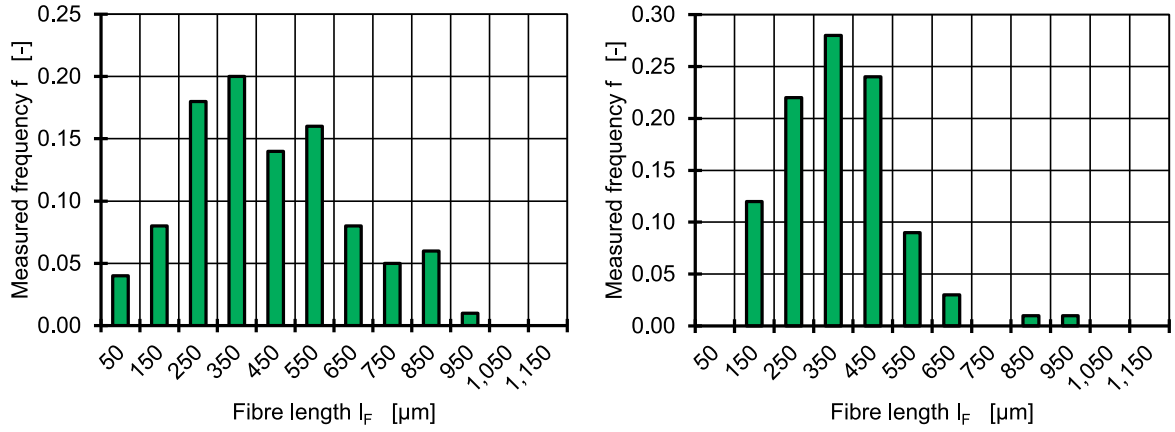

Fig. 5. Fibre length distributions of the PA-GF15 (left) and PA-GF30 (right) taken from [36].

Table 2
Material parameters dependent on the fibre mass content.
Source: Taken from [35].

Name	Mass content	Volume content	Fibre diameter	Orientation degrees		
	ψ [%]	ϕ [%]	d_F [µm]	a_{11} [–]	a_{22} [–]	a_{33} [–]
PA-GF15	15	6.4	13.5	0.507	0.473	0.020
PA-GF30	30	15.2	12.6	0.604	0.354	0.042

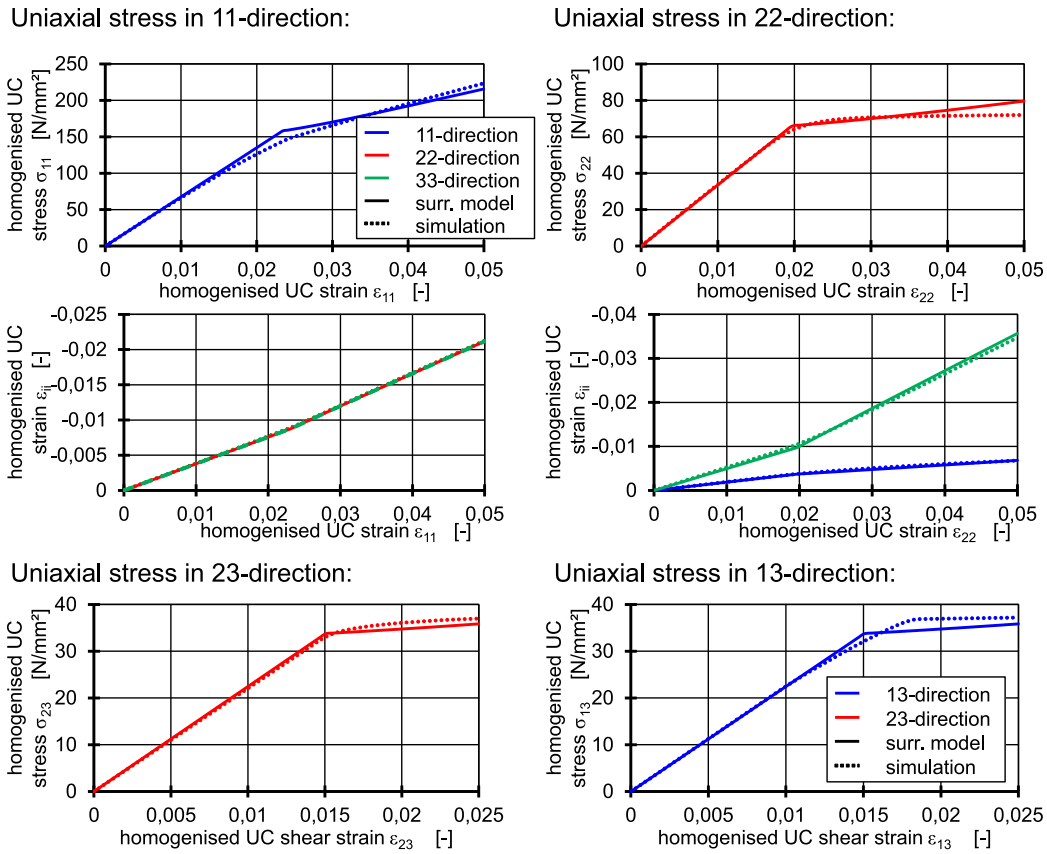

Fig. 6. Surrogate model fits for the FE simulations of four independent uniaxial stress cases in 11, 22, 23 and 13-directions on the PA-GF15 composite with a fibre length of 1150 µm.

Table 3
Representative fibre lengths for the given FLDs.
Source: Taken from [36].

Composite	Number-averaged	Volume-averaged	Stiffness-averaged
PA-GF15	430 μm	532 μm	443 μm
PA-GF30	366 μm	425 μm	372 μm

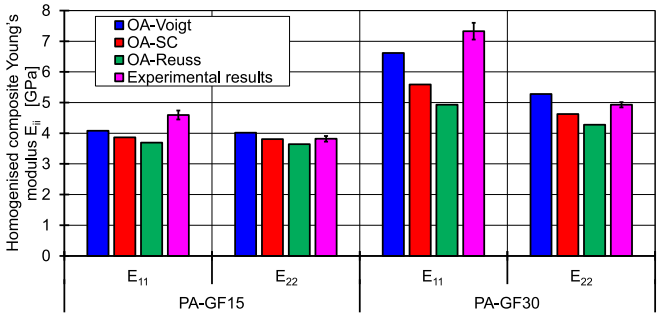

Fig. 7. Linear elastic OA predictions using the fibre length averaging method (method 1) and different interaction assumptions in comparison to experimental results from [35].

Fig. 7, Young's moduli from OA-predictions using the fibre length averaging approach (method 1, see Section 3) are compared to experimental results. Here, the composite moduli are captured well by the model. The anisotropy of the composite is also well-predicted. However, for the 11-direction, the Young's modulus is slightly underestimated by all interaction assumptions. The Young's modulus in 22-direction is well within the range of the predictions and the closest fit is given by the self-consistent interaction. The deviations may be resulting from averaging the orientation distribution over the thickness of the specimen cross section.

Considering the model predictions using method 2, very similar stiffness values are expected. Consequently, a relative assessment is conducted here. The relative composite stiffnesses represented in Fig. 8 are normalised with the OA-prediction from the more detailed method 1. The results of the higher filled PA-GF30 are presented, and similar results are obtained for the PA-GF15. The two different methods result in very similar predictions for all three representative fibre lengths. The maximal deviation from the reference using method 1 is lower than 1%. Comparing the three representative fibre lengths with each other, it is clear, that the volume-averaged fibre length overestimates the composite stiffness in every case. Number- and stiffness-averaged fibre length produce very similar composite stiffness predictions which are very close to the fibre length averaging method. This leads to the conclusion that, considering the linear elastic case (at least, for the studied composites), the use of a representative fibre length is beneficial compared to the fibre length averaging method.

4.3. Elasto-plastic results

In order to evaluate the two presented methods in the elasto-plastic domain, OA-predictions are obtained for the aforementioned composite materials. First, the PA-GF15 composite is investigated in detail. Fig. 9 presents the OA-predictions using method 1 and considering the three interaction assumptions, together with experimental results. The initial stiffness of the composite is underestimated using the Reuss interaction, which is expected as the Reuss assumption provides a lower bound on the homogenised stiffness. However, it can be observed that the complete stress–strain relation is well captured using both the Voigt and the SC interactions. It is only noticed that for high strain values, the trends of experimental results and OA-predictions differ from each other. This discrepancy at larger strains could be attributed to damage occurring in the composite during testing, which is not incorporated in the OA model. Another reason could be the simplifications on which the model is based. The UC simulations do not consider fibre–fibre interactions. Hence, a statistical distribution of matrix yielding cannot be guaranteed.

The effect of different trajectories of the stress-response for larger strains becomes more apparent when considering the higher volume content material, PA-GF30 (see Fig. 10). Here also, the initial stress strain propagation in the experiments is captured very well by the OA-model, especially by the Voigt and the SC interaction assumptions, which match each other very closely. However, due to the negligence of damage occurring for higher strains, the models in the current paper overestimate the homogenised stress response at around 3% strain for the Voigt and SC interaction assumption and 4% strain considering the Reuss interaction assumption.

This shows some of the limitations of the proposed model. First, since no damage mechanism is introduced, the model is only capable of predicting the stress response of the composite in the elastic domain and the initial range of inelastic regime. Second, due to the simplification regarding fibre–fibre interactions, the prediction accuracy of the proposed method may be reduced for very high fibre content values. This is because higher fibre contents increase the probability for effects from fibre–fibre interactions. However, it should be mentioned that higher fibre contents than 30%, as investigated in this study, are not commonly used in SFRCs due to the processability of the material. For the investigated fibre contents, the models give a reasonably good estimation of the actual material response.

Another effect not represented in the model predictions is the layered structure of the FOD in thickness direction of the specimen cross section. Using an averaged fibre orientation distribution disregards this layer structure and all associated interaction mechanisms. The micromechanical model considers a local configuration of the material morphology at a specific location. For a better representation of the layered orientation structure, a coupled multi-scale approach, as proposed in [27], should be applied.

For comparing the predicted behaviour using the simplified approach with method 2, these are compared with the more sophisticated method 1 on the PA-GF15 material using the Voigt assumption. The results are presented in Fig. 11. The four predictions match each other closely. Especially the number and the stiffness-averaged fibre length (using method 2) give a very good estimation of the predicted behaviour in the more detailed model (method 1). Using the volume-averaged fibre length, the stress response is slightly overestimated, especially in the elasto-plastic domain. However, the prediction differences are generally very small and do not lead to a significantly lower prediction accuracy of the material response. In Table 4 the average deviation of using the representative fibre length (method 2) compared to method 1 are given for all three interaction assumptions on the PA-GF15 material. It is seen, that for all interaction assumptions the average deviation is very small. In fact, the maximum deviation from the predictions obtained with method 2 does not exceed 3% for any of the three representative fibre lengths. This is also the case for the PA-GF30 material. The average deviation of the models using method 2 from the fibre length averaging model are presented in Table 5. Consequently, it can be stated that using the representative fibre length does not result in a significant loss of prediction accuracy in comparison to the fibre length averaging method. Considering the much higher computational costs of the more sophisticated method 1, it is clear that also for elasto-plastic OA model, using a single representative fibre length is beneficial. The required computational time scales linearly with the number of fibre length classes considered. In this case, a factor 10 was obtained compared to method 2.

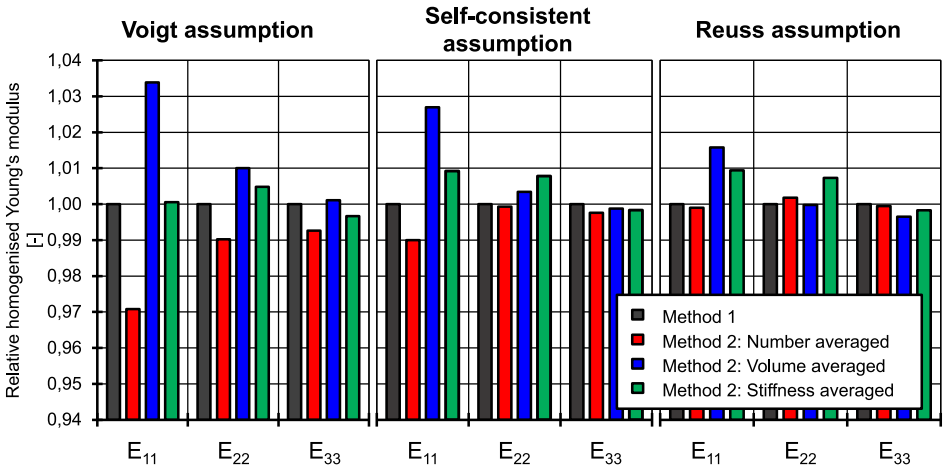

Fig. 8. Relative composite stiffness predictions using method 2 for the three interaction assumptions for the PA-GF30 composite.

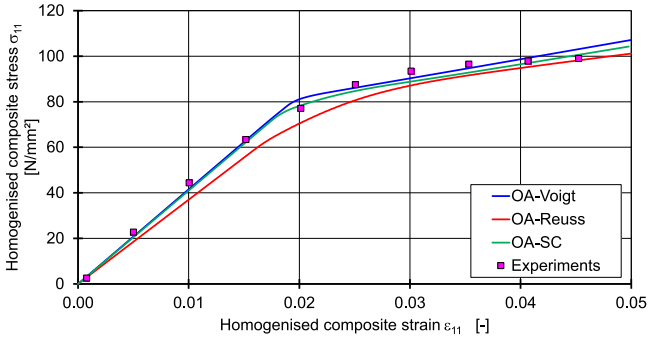

Fig. 9. Elasto-plastic OA predictions for PA-GF15 using method 1 compared to experimental results taken from [35].

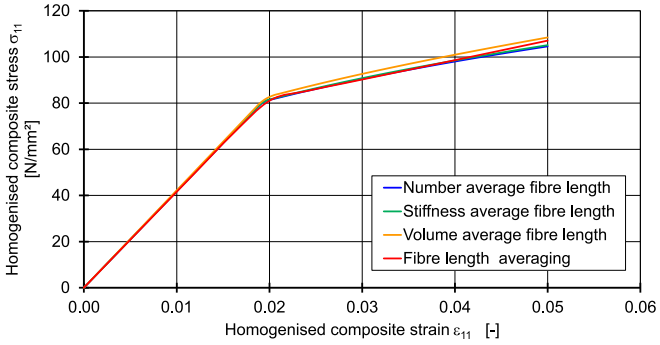

Fig. 11. Comparison of OA prediction using method 2 and method 1 for the PA-GF15 using the Voigt interaction assumption.

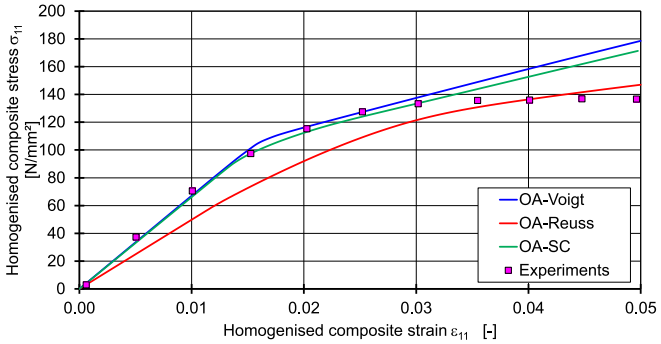

Fig. 10. Elasto-plastic OA predictions for PA-GF30 using method 1 compared to experimental results [36].

Table 4
Average prediction errors of OA-predictions using method 2 compared to predictions obtained from method 1 for the PA-GF15 material.

Interaction assumption	l_F	OA-Voigt	OA-Reuss	OA-SC
Average absolute deviation	[μm]	[%]	[%]	[%]
Number-averaged fibre length	430	0.59	1.04	0.51
Stiffness-averaged fibre length	443	0.62	1.01	0.60
Volume-averaged fibre length	532	1.98	2.21	1.94

Table 5
Average prediction errors of OA-predictions using method 2 compared to predictions obtained from method 1 for the PA-GF30 material.

Interaction assumption	l_F	OA-Voigt	OA-Reuss	OA-SC
Average absolute error	[μm]	[%]	[%]	[%]
Number-averaged fibre length	366	0.61	0.46	0.62
Stiffness-averaged fibre length	372	0.61	0.45	0.66
Volume-averaged fibre length	425	2.65	1.21	2.59

5. Conclusions

Two methods for considering fibre length distributions in an Orientation Averaging method for predicting linear elastic and elasto-plastic response of SFRC were investigated. For the first method, an additional averaging scheme (over different fibre lengths) was introduced, which considers the mechanical response of different fibre lengths taking into account their relative frequency of occurrence. The second method initially reduces the fibre length distribution into a single representative fibre length using different weighting methods. A stiffness-averaged fibre length was introduced, which considers the fibre-length-dependent unidirectional stiffness as a weighting factor.

Both presented methods showed good prediction capabilities of the homogenised composite response. However, there are limitations to the capabilities of the two-step Orientation Averaging model given by the fact that the model simplifies the effect of fibre–fibre interactions and considers no damage mechanism. Therefore, the model predictions start to deviate from experimentally observed data at high strains. Comparing the two methods, the predicted stress–strain relations do not show any significant differences. Hence, for the considered material behaviour, the method using a single representative fibre length is preferred due its computational benefits. Considering the investigated representative fibre lengths, the closest predictions to the method using the additional averaging scheme could be found using number- and stiffness-averaged fibre lengths. The stiffness-averaged fibre length gives a physically based approach and is found to be the preferred method.

CRediT authorship contribution statement

N. Mentges: Data curation, Formal analysis, Investigation, Methodology, Software, Validation, Visualization, Writing – original draft. **H. Çelik:** Methodology, Supervision, Writing – review & editing. **C. Hopmann:** Funding acquisition, Writing – review & editing. **M. Fagerström:** Conceptualization, Funding acquisition, Methodology, Resources, Supervision, Writing – review & editing. **S.M. Mirkhalaf:** Conceptualization, Funding acquisition, Methodology, Project administration, Supervision, Writing – original draft, Writing – review & editing.

Declaration of competing interest

The authors declare that they have no known competing financial interests or personal relationships that could have appeared to influence the work reported in this paper.

Data availability

No additional data to the datasets presented in the manuscript was used for the research described in the article.

Acknowledgement

S.M. Mirkhalaf is grateful for the financial support from the Swedish Research Council (VR grant: 2019-04715). M. Fagerström gratefully acknowledges the financial support through Vinnova's strategic innovation programme LIGHTer (LIGHTer Academy grant no. 2020-04526).

Appendix A. Surrogate model parameters

A.1. PA-GF15

See Tables A.1 and A.2.

A.2. PA-GF30

See Tables A.3 and A.4.

Table A.1
Model parameters and objective function values for the calibration of the surrogate model on simulations of discrete fibre lengths of PA GF15.

l_F	ϵ_{fit}^{el}	ϵ_{fit}^{pl}	E	ν	k	σ_y	R	κ_1	κ_2	κ_3
[µm]	[–]	[–]	[MPa]	[–]	[–]	[N/mm^2]	[–]	[–]	[–]	[–]
50	3.264×10^{-2}	3.845×10^{-2}	2993	0.3046	1.300	61.33	1.463	20.38	0.000	0.0000
150	3.748×10^{-2}	2.735×10^{-2}	3041	0.3225	1.504	64.24	2.333	38.66	68.24	0.0066
250	2.420×10^{-2}	1.834×10^{-2}	3052	0.3347	1.609	65.13	3.818	30.70	943.0	22.12
350	1.657×10^{-2}	9.410×10^{-3}	3059	0.3441	1.648	65.52	5.402	25.70	1008	125.4
450	1.186×10^{-2}	6.227×10^{-3}	3066	0.3515	1.661	65.77	6.618	23.73	1074	135.9
550	8.787×10^{-3}	5.382×10^{-3}	3072	0.3576	1.664	65.91	7.525	23.48	1116	182.1
650	6.659×10^{-3}	5.123×10^{-3}	3077	0.3626	1.662	65.98	8.220	23.11	1205	194.2
750	5.078×10^{-3}	5.052×10^{-3}	3082	0.3669	1.657	66.05	8.834	22.62	1245	212.8
850	3.922×10^{-3}	5.012×10^{-3}	3086	0.3705	1.652	66.10	9.374	22.71	1227	316.1
950	3.055×10^{-3}	5.026×10^{-3}	3089	0.3737	1.647	66.15	9.747	22.41	1316	328.5
1050	2.367×10^{-3}	5.087×10^{-3}	3091	0.3764	1.641	66.21	10.20	21.65	1316	328.5
1150	1.901×10^{-3}	5.132×10^{-3}	3094	0.3788	1.636	66.21	10.58	22.40	1254	392.5

Table A.2
Model parameters and objective function values for the calibration of the surrogate model on simulations of representative fibre lengths of PA GF15.

l_F	ϵ_{fit}^{el}	ϵ_{fit}^{pl}	E	ν	k	σ_y	R	κ_1	κ_2	κ_3
[µm]	[–]	[–]	[MPa]	[–]	[–]	[N/mm^2]	[–]	[–]	[–]	[–]
430	4.139×10^{-4}	1.490×10^{-2}	3119	0.3971	1.487	65.74	6.396	38.72	0.000	110.8
443	4.247×10^{-4}	1.439×10^{-2}	3119	0.3973	1.489	65.76	6.510	38.87	0.000	110.9
532	4.656×10^{-4}	1.198×10^{-2}	3121	0.3983	1.501	65.86	7.241	36.14	250.0	112.5

Table A.3
Model parameters and objective function values for the calibration of the surrogate model on simulations of discrete fibre lengths of PA GF30.

l_F	ϵ_{fit}^{el}	ϵ_{fit}^{pl}	E	ν	k	σ_y	R	κ_1	κ_2	κ_3
[µm]	[–]	[–]	[MPa]	[–]	[–]	[N/mm^2]	[–]	[–]	[–]	[–]
50	9.161×10^{-3}	6.879×10^{-3}	3620	0.3543	1.536	62.15	2.690	38.40	0.000	0.000
150	4.807×10^{-3}	6.603×10^{-3}	3602	0.3701	1.940	63.97	7.794	44.78	88.60	86.83
250	3.306×10^{-3}	6.891×10^{-3}	3601	0.3768	2.063	64.40	12.01	38.03	1033	208.8
350	2.541×10^{-3}	7.606×10^{-3}	3604	0.3822	2.107	64.56	15.85	34.71	1285	138.7
450	2.198×10^{-3}	8.152×10^{-3}	3608	0.3866	2.122	64.66	19.22	33.81	1267	1948
550	2.238×10^{-3}	8.867×10^{-3}	3615	0.3932	2.101	64.72	22.22	33.62	1248	1117
650	2.423×10^{-3}	9.199×10^{-3}	3617	0.3958	2.102	64.76	24.91	33.65	1188	1412
750	2.682×10^{-3}	9.514×10^{-3}	3619	0.3982	2.098	64.80	27.20	33.77	1156	1614
850	2.975×10^{-3}	9.887×10^{-3}	3621	0.4001	2.093	64.73	29.28	35.43	1031	1971
950	3.278×10^{-3}	1.008×10^{-2}	3622	0.4018	2.088	64.77	31.25	35.82	964.4	1657
1050	3.598×10^{-3}	1.033×10^{-2}	3624	0.4034	2.081	64.76	32.99	36.11	919.9	2000
1150	3.891×10^{-3}	1.049×10^{-2}	3625	0.4047	2.077	64.80	34.65	36.22	874.8	1647

Table A.4
Model parameters and objective function values for the calibration of the surrogate model on simulations of representative fibre lengths of PA GF30.

l_F	ϵ_{fit}^{el}	ϵ_{fit}^{pl}	E	ν	k	σ_y	R	κ_1	κ_2	κ_3
[µm]	[–]	[–]	[MPa]	[–]	[–]	[N/mm^2]	[–]	[–]	[–]	[–]
366	2.257×10^{-2}	7.954×10^{-2}	3543	0.3377	2.428	64.58	16.06	38.22	1417	457.5
372	2.255×10^{-2}	8.009×10^{-2}	3542	0.3376	2.434	64.61	16.26	37.83	1470	28.32
425	2.253×10^{-2}	8.278×10^{-2}	3542	0.3379	2.463	64.64	17.71	37.35	1652	153.2

References

[1] Fu S, Lauke B, Mai Y. Science and engineering of short fibre-reinforced polymer composites. Elsevier; 2019.

[2] Mirkhalaf SM, Eggels E, Anantharanga AT, Larsson F, Fagerström M. Short fiber composites: computational homoginisation vs. orientation averaging. In: ICCM22. Melbourne, Autralia; 2019.

[3] Tucker III Charles L, Liang E. Stiffness predictions for unidirectional short-fiber composites: Review and evaluation. Compos Sci Technol 1999;59(5):655–71.

[4] Phelps JH. Processing-microstructure models for short- and long-fibre thermoplastic composites [Ph.D. thesis], Urbana: University of illinois; 2009.

[5] Osswald TA, Menges G. Materials science of polymers for engineers. 3. Aufl.. München: Carl Hanser Verlag; 2012.

[6] Chin W, Liu H, Lee Y. Effects of fiber length and orientation distribution on the elastic modulus of short fiber reinforced thermoplastics. Polym Compos 1988;9:27–35.

[7] Mori T, Tanaka K. Average stress in matrix and average elastic energy of materials with misfitting inclusions. Acta Metall 1973;21(5):571–4.

[8] Pierard O, Friebel C, Doghri I. Mean-field homogenization of multi-phase thermo-elastic composites: A general framework and its validation. Compos Sci Technol 2004;64(10):1587–603.

[9] Advani SG, Tucker CL. The use of tensors to describe and predict fiber orientation in short fiber composites. J Rheol 1987;31(8):751–84.

[10] Breuer K, Stommel M, Korte W. Analysis and evaluation of fiber orientation reconstruction methods. J Compos Sci 2019;3(67).

[11] Al-Qudsi A, Çelik H, Neuhaus J, Hopmann C. A comparative study between fiber orientation closure approximations and a new orthotropic closure. Polym Compos 2022.

[12] Halpin JC. Stiffness and expansion estimates for oriented short fiber composites. J Compos Mater 1969;3:732–4.

[13] Lusti H. Direct numerical predictions for the elastic and thermoelastic properties of short fibre composites. Compos Sci Technol 2002;62(15):1927–34.

[14] Müller V, Brylka B, Dillenberger F, Glöckner R, Kolling S, Böhlke T. Homogenization of elastic properties of short-fiber reinforced composites based on measured microstructure data. J Compos Mater 2016;50(3):297–312.

[15] Nguyen BN, Bapanapalli SK, Holbery JD, Smith MT, Kunc V, Frame BJ, et al. Fiber length and orientation in long-fiber injection-molded thermoplastics: Part I: Modeling of microstructure and elastic properties. J Compos Mater 2008;42(10):1003–29.

[16] Lee DJ, Hwang SH, Song YS, Youn JR. Statistical modeling of effective elastic modulus for multiphased hybrid composites. Polym Test 2015;41:99–105.

[17] Fu SY, Lauke B. The elastic modulus of misaligned short-fiber-reinforced polymers. Compos Sci Technol 1998;58(3):389–400.

[18] Hine PJ, Lusti HR, Gusev AA. Numerical simulation of the effects of volume fraction, aspect ratio and fibre length distribution on the elastic and thermoelastic properties of short fibre composites. Compos Sci Technol 2002;62:1445–53.

[19] Hine PJ, Lusti HR, Gusev AA. On the possibility of reduced variable predictions for the thermoelastic properties of short fibre composites. Compos Sci Technol 2004;64:1081–8.

[20] Breuer K, Stommel M. RVE modelling of short fiber reinforced thermoplastics with discrete fiber orientation and fiber length distribution. SN Applied Sciences 2019;2.

[21] Modniks J, Andersons J. Modeling elastic properties of short flax fiber-reinforced composites by orientation averaging. Comput Mater Sci 2010;50(2):595–9.

[22] Sasayama T, Okabe T, Aoyagi Y, Nishikawa M. Prediction of failure properties of injection-molded short glass fiber-reinforced polyamide 6,6. Composites A 2013;52:45–54.

[23] Notta-Cuvier D, Lauro F, Bennani B. An original approach for mechanical modelling of short-fibre reinforced composites with complex distributions of fibre orientation. Composites A 2014;62:60–6.

[24] Mirkhalaf SM, van Beurden TJH, Ekh M, Larsson F, Fagerström M. An FE-based orientation averaging model for elasto-plastic behavior of short fiber composites. Int J Mech Sci 2022;219:107097.

[25] Mirkhalaf SM, Eggels EH, van Beurden TJH, Larsson F, Fagerström M. A finite element based orientation averaging method for predicting elastic properties of short fiber reinforced composites. Composites B 2020;202.

[26] Castricum B, van Beurden TJH, Mirkhalaf M, Fagerström M, Larsson F. A hierarchical coupled multi-scale model for short fiber composites. In: 14th WCCM-ECCOMAS congress. CIMNE; 2021.

[27] Castricum BA, Fagerström M, Ekh M, Larsson F, Mirkhalaf SM. A computationally efficient coupled multi-scale model for short fiber reinforced composites. Composites A 2022;163:107233.

[28] Hori M, Nemat-Nasser S. Double-inclusion model and overall moduli of multi-phase composites. Mech Mater 1993;14(3):189–206.

[29] Hori M, Nemat-Nasser S. Double-inclusion model and overall moduli of multi-phase composites. J Eng Mater Technol 1994;116(3):305–9.

[30] Runesson K, Steinmann P, Ekh M, Menzel A. Constitutive modeling of engineering materials: Theory and computation. Volume I general concepts and inelasticity. 2006.

[31] Bingham C. An antipodally symmetric distribution on the sphere. Ann Statist 1974;2(6):1201–25.

[32] Eshelby JD. The determination of the elastic field of an ellipsoidal inclusion, and related problems. Proc R Soc Lond Ser A 1957;241(1226):376–96.

[33] Mortazavian S, Fatemi A. Effects of fiber orientation and anisotropy on tensile strength and elastic modulus of short fiber reinforced polymer composites. Composites B 2015;72:116–29.

[34] Karsli NG, Aytac A, Deniz V. Effects of initial fiber length and fiber length distribution on the properties of carbon-fiber-reinforced-polypropylene composites. J Reinf Plast Compos 2012;31(15):1053–60.

[35] Holmström PH, Hopperstad OS, Clausen AH. Anisotropic tensile behaviour of short glass-fibre reinforced polyamide-6. Compos C: Open Access 2020;2.

[36] Holmström PH. Data for: Anisotropic tensile behaviour of short glass-fibre reinforced polyamide-6. Mendeley; 2020.

[37] Schürmann H. Konstruieren mit Faser-Kunststoff-Verbunden. VDI-Buch, 2., bearbeitete und erweiterte Auflage. Berlin, Heidelberg: Springer-Verlag Berlin Heidelberg; 2007.

[38] ISO International Organization for Standardization. Metallic materials - tensile testing: Part 1: Method of test at room temperature, no. 6892-1. Vernier, CH: ISO International Organization for Standardization; 2019.